Summer 2015

Nonlinear optical response in graphene

Xin Jin
University of Iowa

NONLINEAR OPTICAL RESPONSE IN GRAPHENE

by

Xin Jin

A thesis submitted in partial fulfillment of the
requirements for the Master of Science degree
in Electrical and Computer Engineering
in the Graduate College of
The University of Iowa

August 2015

Thesis Supervisor: Professor David R. Andersen

Graduate College
The University of Iowa
Iowa City, Iowa

CERTIFICATE OF APPROVAL

_____

MASTER'S THESIS

_____

This is to certify that the Master's thesis of

Xin Jin

has been approved by the Examining Committee
for the thesis requirement for the Master of
Science degree in Electrical and Computer
Engineering at the August 2015 graduation.

Thesis Committee:_____
David R. Andersen, Thesis Supervisor

_____
Er-Wei Bai

_____
Fatima Toor

To my family.

ACKNOWLEDGMENTS

First and foremost, I would like to express my deepest gratitude to my advisor: David R. Andersen, for his constant encouragement throughout my graduate program. His patience, valuable comments, guidance and support helped me completing this thesis smoothly.

I would like to thank my thesis committee members: Prof. Er-Wei Bai and Prof. Fatima Toor, for serving my committee members, and giving insightful comments on my thesis. I would also like to thank my colleague Yichao Wang for the insightful discussion.

Last but not the least, I would like to thank my parents for supporting and encouraging me throughout my entire life.

ABSTRACT

Graphene, a newly discovered carbon based material, is predicted to have a strong nonlinear electromagnetic response over a broad spectral range. Its unique carrier transport and terahertz properties have gained ample attention. Recently, it has been demonstrated that graphene has an extraordinarily high nonlinear response with third-order susceptibility $\chi^3 \sim 10^{-7}$ esu, which is 10^5 times higher than that of silicon.

In this thesis, we examine the nonlinear response of electron dynamics in graphene using the newly derived optical Bloch equations. The thesis is divided into three sections. In the first part, we provide an overview of the derivation of the extended optical Bloch equations from the time-dependent Dirac equations. Then, we use these derived optical Bloch equations to demonstrate the coupling of light and field interaction in graphene, and the generation of photon echo signal. Next, we describe the nonlinear response in graphene in terms of the current density, and we show that the enhanced interband dynamics reduces nonlinearity in the electric current. Finally, we illustrate that the strong interplay between the interband and intraband dynamics leads to large harmonic generations, where harmonics of up to 13^{th} order are generated.

PUBLIC ABSTRACT

Nonlinear optical phenomena in materials are significant for the development of useful photonic applications. Studying these effects not only would improve the performance of the nonlinear materials in applications with their wide transparency range, fast response, and high damaging threshold, but also would push the industries to develop more advanced techniques for the fabrication and growth of artificial materials. Therefore, the search for and study of nonlinear material is highly desirable.

Graphene, a newly discovered carbon-based material, is predicted to have strong nonlinear electromagnetic response over a broad spectral range. The purpose of this thesis is to examine the nonlinear optical effects in graphene, including light and field interaction, photon echo generation, current density and harmonic generation, using the newly derived optical Bloch equations.

TABLE OF CONTENTS

LIST OF FIGURES

Figure

CHAPTER I

INTRODUCTION

Graphene

Background

Graphene is a material in a two-dimensional single atomic layer and made of carbon atoms bonded in a honeycomb lattice (shown in Figure 1.1). Graphene is the basic structure of graphite, carbon nanotubes, fullerenes and diamond (shown in Figure 1.2). Since its discovery by scientists Andre Geim and Kostya Novoselov in 2004, it is predicted that graphene will bring a new revolution to the current carbon-based electronics on account of its remarkable physical properties. Graphene is the strongest (stronger than diamond) and thinnest (thinner than a paper) material that has ever been known. In addition, graphene is much more flexible than silicon, which is the most widely used material in the electronic world. And it was reported that graphene could be stretched by 20% while silicon could only be stretched by 1% [1]. Moreover, it has been observed that graphene conducts heat and electricity with great efficiency. Additionally, graphene will provide scientists an excellent model to study relativistic quantum phenomena [2,3] such as the quantum Hall effect [4] in condensed matter material.

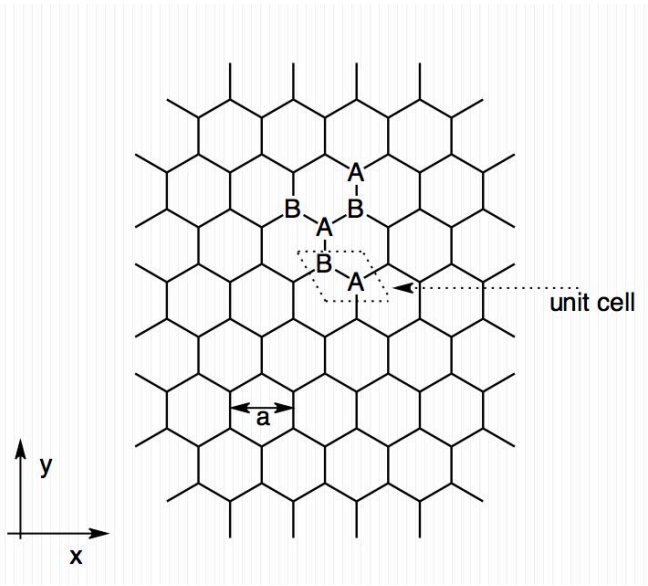

Figure 1.1. The hexagonal honeycomb lattice of graphene with the primitive vector a = 2.46 Å. The unit cell consists of two sublattices: A and B.

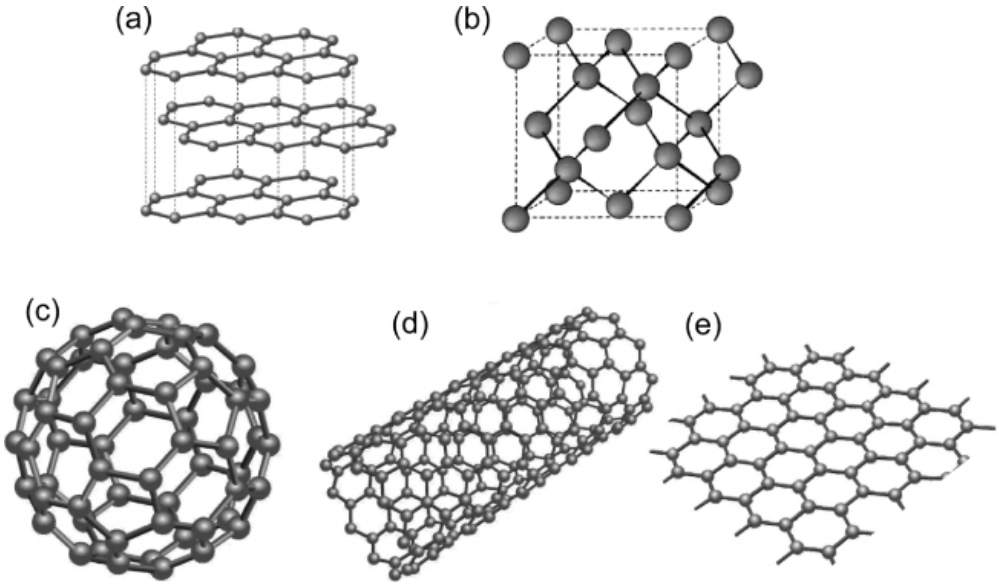

Figure 1.2. (a) Graphite: stack of graphene sheets; (b) Diamond: cubic; (c) Fullerenes: closed cage of carbon; (d) Carbon nanotube: rolled-up sheets of graphene; (e) Graphene. From Ref. [5]

Structure of graphene

In graphene, there are two carbon atoms per unit cell, displayed as A and B in Figure 1.1. Each carbon atom, which is the sixth element (of periodic table) with a total of 6 electrons, has the electron configuration of $1s^2 2s^2 2p^2$. Here one 2s orbital per carbon in graphene is combined with the $2p_x$ and $2p_y$ to form three sp2 orbitals. And the sp2 orbital of each carbon is then bonded with the adjacent sp2 orbital forming a strong covalent σ band that is 1.42 Å long. The remaining $2p_z$ orbital, which is perpendicular to the planar structure, forms a covalent π band with the

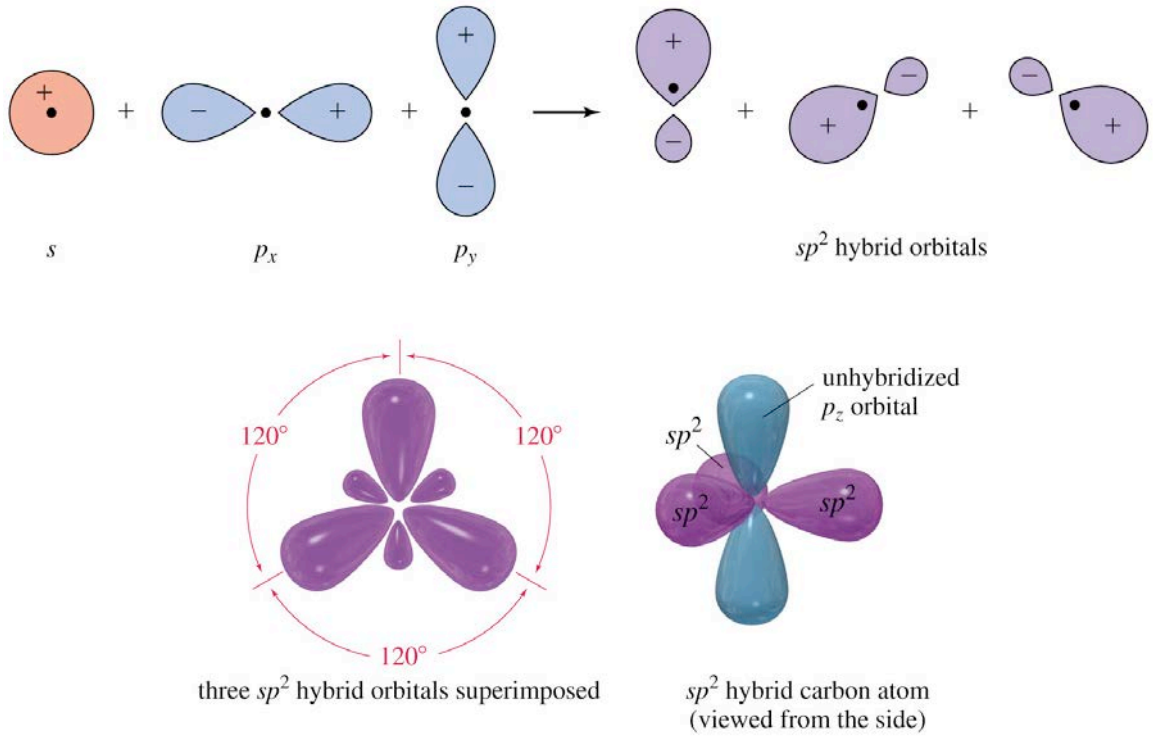

Figure 1.3. The bonding process of graphene structure: one 2s orbital is combined with the $2p_x$ and $2p_y$ to form three sp2 orbitals, and the remaining $2p_z$ orbital is perpendicular to the planar structure. From Ref. [6].

neighboring carbon atom. In addition, the π band is half-filled, and it is responsible for the conductivity of graphene with an extra electron from each p orbital. The bonding process of graphene structure is illustrated in Figure 1.3. The σ and π bands in graphene form the Fermi surface, which is characterized as six double cones as shown in Figure 1.4. And in the undoped environment, the corners (depicted as two Fermi points: K and K', and they are also displayed on the first Brillouin zone of graphene in Figure 1.5) of these six double cones are the Fermi level of graphene, and are separating conduction and valence bands. According to this band structure, graphene is a zero gap semiconductor. On the other hand, it means that the density state of the intrinsic graphene is zero at the Fermi level. As will be discussed in detail later, the Fermi level of graphene can be modified by applying an electric field, where graphene becomes either p-doped or n-doped. In general, the electrical conductivity for doped graphene is very high compared to the undoped graphene. The π band electronic dispersion of graphene at six corners of the Brillouin zone is found to be linear, $\varepsilon_p = \pm v_F|p|$, where v_F = c/30 is the electron Fermi velocity, c is the speed of the light, p is the charge carrier momentum and $\pm$ represents conduction and valence bands [7]. Because of this linear relation between the energy and the momentum, electrons propagating through graphene behave as massless Dirac fermion [8], which have attracted a great interest in the development of the graphene-based electronic devices.

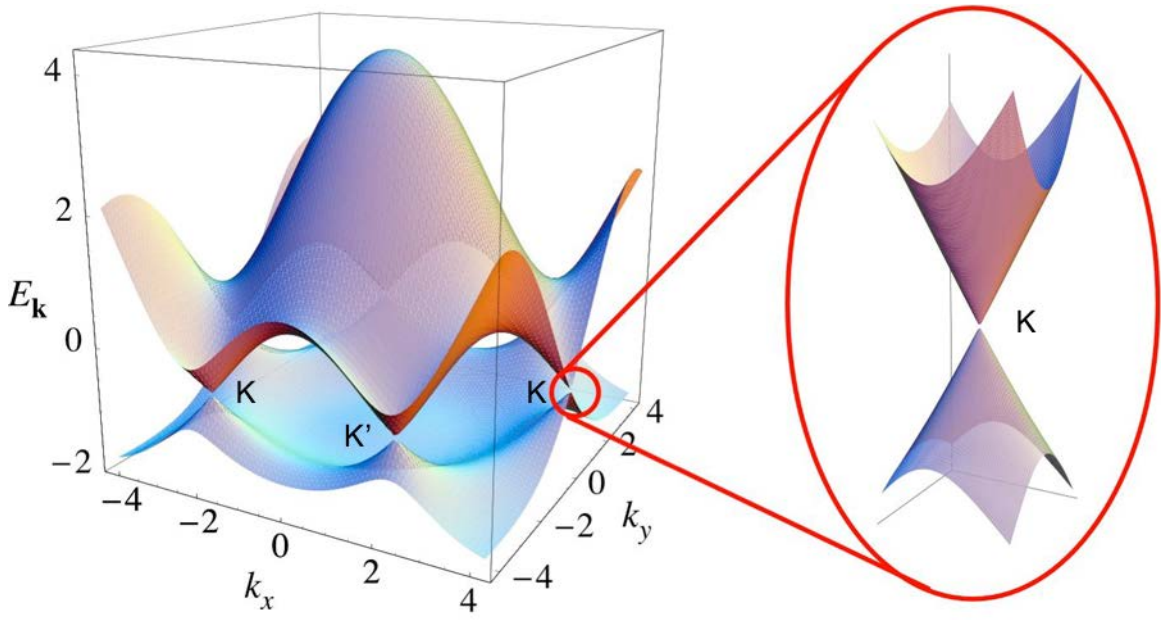

Figure 1.4. Band structure of graphene. There are six Dirac points, but only two of them are non-equivalent, and they are denoted as K and K'. The conduction and valence band are touching at the Dirac points. From Ref. [9].

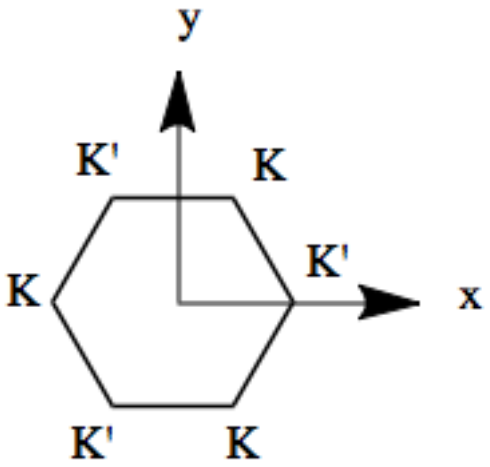

Figure 1.5. The first Brillouin zone of graphene with two non-equivalent Dirac points denoted as K and K'. The points K and K' are the touching points of the Energy bands.

Nonlinearity in graphene

Not only has linear dispersion of electron energy of graphene attracted lots of fundamental research and the development of numerous devices, but its fascinating optical property would also open a new door for exploring a wide spectrum of applications ranging from optoelectronics [10], photonics [10], sensors [11], and biodevices [12,13]. Currently, lots of nonlinear optics phenomena of graphene have been extensively studied and experimented, including harmonic generation [14,15,16], optical rectification [7], photon drag effect [17,18], frequency mixing [19], and coherently controlled ballistic charge currents [20]. And most of these processes would lead to the development of applications like all-optical switching [21,22,23], optical power limiting [24,25], terahertz transistors [26], and fast optical communication [27,28].

In general, nonlinear optics studies the behavior of light traveling through nonlinear media, where matter interacts with the incident radiation field and responds in way that is not linearly proportional to the incident radiation field. An example of this kind of phenomena would be the second harmonic generation in which two waves with exact frequency, which interact with a nonlinear media, are superimposed to generate a new wave that has twice the energy and frequency as the initial waves ($w_{photon} + w_{photon} = 2w_{photon}$). [29] A schematic displaying the second harmonic generation process is shown in figure 1.6. Typically, the nonlinear response in all materials can only be observed when the incident light has

sufficiently high intensity such as lasers. And for incident light with low optical intensity, nonlinear effects in materials normally become very weak. The nonlinear response in all materials can be characterized mathematically by expanding the dielectric polarization density $\tilde{p}(t) = \epsilon_0 \chi^1 \tilde{E}(t)$ (where $\tilde{p}(t)$ is the induced polarization in the media, $\tilde{E}(t)$ is the field strength of the incident light, ϵ_0 is the permittivity of free space, and χ is the linear susceptibility) as a power series in the field strength $\tilde{E}(t)$ as follows :

$$\tilde{P}(t) = \epsilon_0[\chi^1 \tilde{E}(t) + \chi^2 \tilde{E}^2(t) + \chi^3 \tilde{E}^3(t) + \cdots] \qquad (1)$$

Here first term χ^1 is linear susceptibility. χ^2 and χ^3 are second- and third-susceptibilities, and they describe the nonlinear effects including second and third

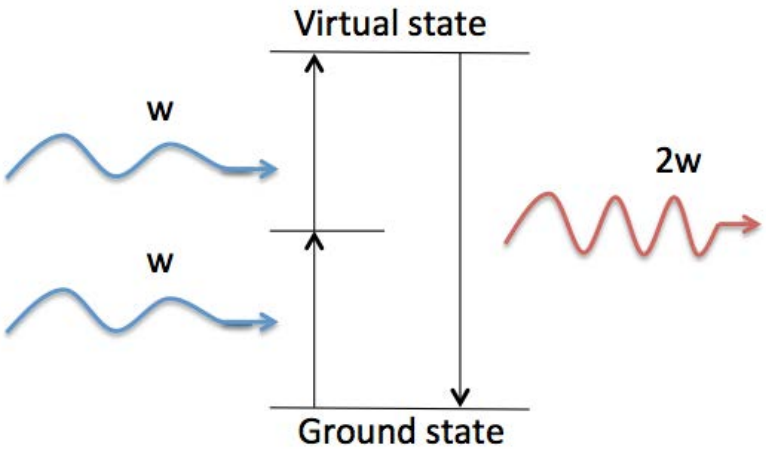

Figure 1.6. Schematic of the second harmonic generation. As shown, two waves with exact frequency interact with media, and generate an output wave that has twice the frequency as the initial wave.

harmonic generation and the intensity-dependent refractive index [30]. Several important criteria have to be considered when it comes to selecting materials for applications of nonlinear optics, including having large susceptibility, highly transmitting at all wavelengths of interest, being highly resistant to laser damage, having fast temporal response, and being chemically stable [30]. In the last decades, extensively studying the effects of nonlinear optical material has helped us improve the performance of the nonlinear optical materials in applications with their wide transparency range, fast response, and high damaging threshold. Moreover, it pushes the industries to develop more advanced techniques for the fabrication and growth of artificial materials.

Nonlinear properties of graphene can be theoretically studied by applying an electric field to the media, and observe the nonlinear dynamics in the induced electric currents. In general, there are three regimes of optical excitation in the whole process: direct and indirect interband transition, and indirect intraband transitions (these three transitions are shown in Figure 1.7(a), (b), (c), respectively) [7]. And these three transitions are determined by the relationship between the Fermi (E_F) and photon ($\hbar W$) energies. For example, when the condition is $E_F \leq \hbar W \leq 2E_F$, indirect interband transition dominates the whole absorption processes. For $\hbar w \leq E_F$, the transition is indirect intraband transition. And for $\hbar W \geq 2E_F$, the transition is indirect intraband transition. In the last decades, extensively studying of interband and intraband transitions in graphene shows that intraband transition dominates for the long wavelengths (THz range) with conductivity exhibiting like Drude model, while interband transition dominates for

the short wavelengths (infrared and visible range) with an absorption coefficient of 2.3% [31,32,33]. And recently, devices like photodetectors [34,35], transparent electrons and broadband modulators [36,37] have already been demonstrated using graphene's property of interband transition.

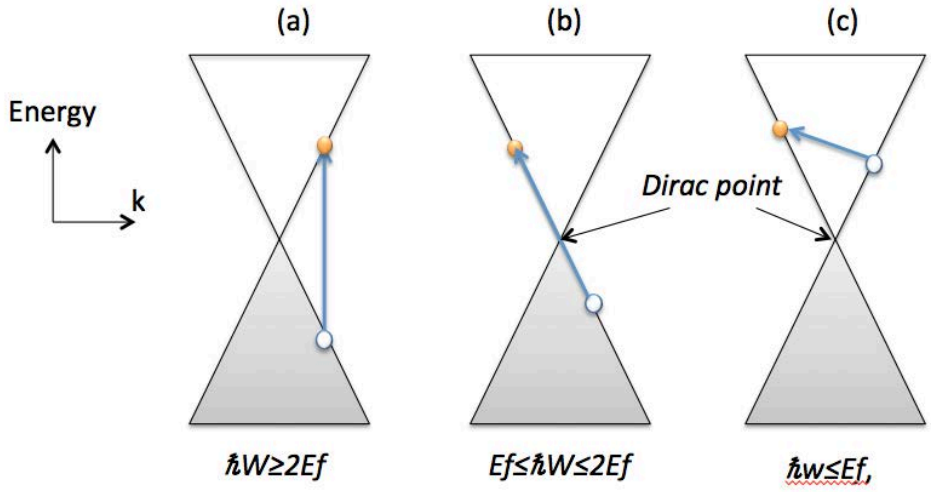

Figure 1.7: Schematic of the optical transitions. (a): direct interband transition;(b) indirect interband transition; (c): indirect intraband transition

Production

Graphene was first produced using the 'scotch tape' technique [38], where bulk graphite was pulled off step by step until a single layer remains. Using this technique not only would produce the most purified and defect-free samples, but also could preserve graphene's remarkable electronic properties. However, this

technique could not be used to produce graphene on a large scale for industrial use purpose. Therefore, new techniques need to be developed in order to produce large-scale, high quality and low cost (currently $200-$900/kg depending on quality and grade [39]) graphene to produce commercial volumes. Until now, there are several methodologies that have already been developed to make graphene in large scale, including chemical vapor decomposition (CVD) [40,41,42], liquid phase exfoliation [43,44], and segregation by heat treatment of carbon-containing substrates [45]. Among these, chemical vapor decomposition by far is the most promising technique to produce large-scale and high quality graphene. In this process, gas molecules (methane and hydrogen) are passing through a reaction chamber constantly, where a reaction is taken place on the surface of the transition metal substrates (like Cupper and Nickel), and leave a thick layer of carbon. The temperature of the chamber plays a key role during the process as it controls what kind of reaction will occur, and it is normally set at ambient temperature. And when the reaction chamber cools down, the carbon on the transition metal substrates will crystalizes into a layer of graphene [40]. Although CVD has been the most popular technique to produce graphene, it has flaws, one of which is that the final product of graphene might be contaminated or ruined when it is peeled off from the metal substrates. But a recent discovery by the researchers at the University of Groningen in the Netherlands has resolved this problem [46]. What they discovered was that graphene formed a film layer on the top of the copper oxide, and, with the help of this protection layer, graphene can be isolated from the copper substrate without even being ruined or contaminated. Furthermore, all its fascinating electronic

properties would be preserved. Even though massive production of graphene is still a big challenge today, with growing research and further understanding of physical properties of graphene, this challenge will be easily overcome in the near future.

Graphene Nanoribbons

Background

Graphene nanoribbons are defined as one-dimensional thin strips of graphene. They inherit most novel optical, electronic, and magnetic properties from graphene. However, due to their special structures, they have some unique properties that graphene does not have such as a tunable band gap [47,48]. In general, there are two kinds of nanoribbons based on the geometry of their edges: armchair and zigzag (structures of armchair and zigzag nanoribbons are shown on Figure 1.8 (a) and (b)). From their structures, one could tell that when the edge of armchair nanoribbons is rolled into cylinder, it forms a zigzag nanotube. And when the edge of zigzag nanoribbons is rolled into cylinder, it forms an armchair nanotube [49,50]. As will be discussed in detail later, the width and chirality of ribbons play important roles in defining the electronic properties of GNRs. For instance, armchair nanoribbons can be either metallic or semiconducting while zigzag nanoribbons are always metallic depending on their width. Researchers have predicted that extensively studying GNRs not only could help explore the nano-scale size and edge

effect in graphene, but also could discover new types of devices such as spin-valves [51,52], nanoribbons switches [53,54], and detectors [55]. And according to recent published papers, graphene nanoribbons have already been successfully used in applications including field-effect transistors [56,57], conductive electrode [58,59], solar cell systems [60,61,62], light emitting diodes [63], P-N junctions [64], and schotkky diodes [65].

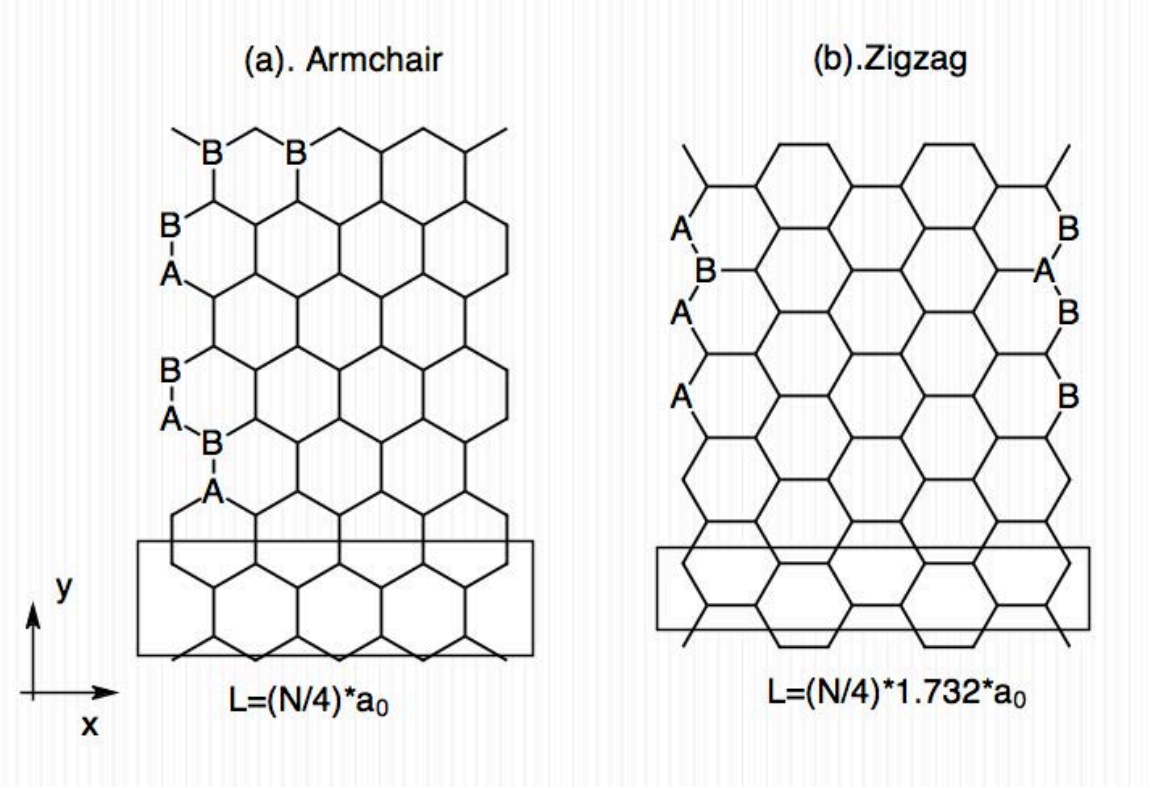

Figure 1.8: (a) The structure of armchair nanoribbons with edge that have two nonequivalent sublattices A and B. (b) The structure of zigzag nanoribbons with edge that either has sublattices A or B.

Armchair nanoribbons

In armchair nanoribbons, there are two nonequivalent atoms forming bonds along its edge (defined as sublattices A and B), as illustrated on figure 1.8 (a). And according to this unique edge structure, the amplitude of wave function vanishes on both sublattices at x=0 and x=L+$a_0/2$ [66]. In our discussion, we choose edges run along the y direction. The unit cell consists of n A-types and n B-types atoms, and the width of the ribbons is related to the number of atoms in the unit cell via equation $L = \frac{N}{4} a_0$ (L is width, N is the number of atoms and a_0 is the graphene lattice constant). As mentioned earlier, the electronic properties of armchair nanoribbons depend strongly on its width with band gap that is inversely proportional to the width and eventually approaches zero when L goes to infinite. In general, with width L = 3P or L = 3P + 1 (where p is an integer), armchair nanoribbons shows semiconducting behavior. And when L = 3P + 2, the system is metallic. For instance, armchair nanoribbons is semiconducting with L =7 and is metallic with L=5. The energy dispersion relation for armchair nanoribbons has been observed, and it is the same as that for graphene, which is expressed as

$$\varepsilon^s(k,\theta) = s\gamma_0\sqrt{1 + 4cos^2(\theta) + 4\cos(\theta)\cos(kl)}, \qquad (2)$$

where s is represented as the conduction and valence bands with signs ± 1, γ_0 is the hopping integral (=3 eV), $l = \frac{\sqrt{3}a_0}{2}$ ($a_0 = 2.46$ Å), k is the wave vector along the edge and θ is the phase that is perpendicular to the edge [67]. Equation 2 shows that

energy of armchair nanoribbons depends on wave vector k and phase angle θ. The energy band structures of armchair nanoribbons can be obtained by slicing the band structure of graphene, as in the case of carbon nanotubes. And as shown in figure 1.9 (a), the Brillouin zone of armchair is only half of that for graphene [67] because of the reflection at the edge of the armchair, and the Dirac point on the Brillouin zone is at (k, θ)=(0, 2π/3).

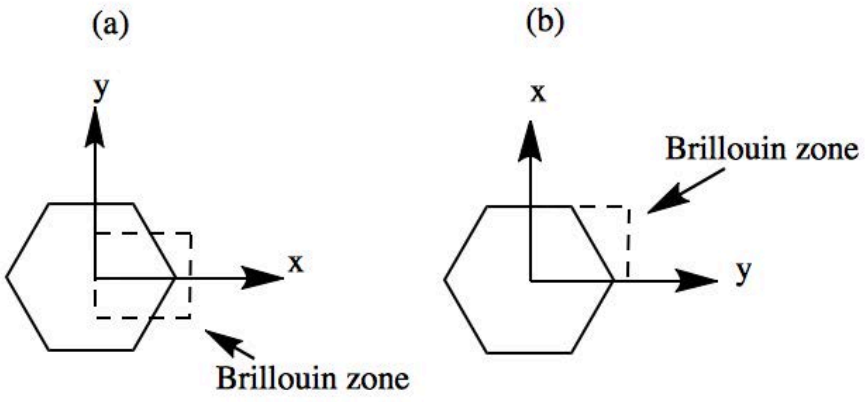

Figure 1.9. (a) The first Brillouin zone of armchair nanoribbons. (b) The first Brillouin zone of zigzag nanoribbons.

Zigzag nanoribbons

In zigzag nanoribbons, atoms along the edge are of the same sublattices (denoted as A on the left edge or B on the right edge of the figure), as illustrated in figure 1.7 (b). Due to edge differences, zigzag nanoribbons exhibits all aspects of

properties differently from armchair nanoribbons. For example, when a polarized light is applied parallel to the edges of both ribbons, the interband transitions in zigzag nanoribbons are indirect transitions while they happen to be direct transition in armchair nanoribbons [66]. As pointed out earlier, zigzag nanoribbons are always metallic because they have a zero-energy localized state at the Fermi level. The width of the ribbon can be expressed via equation $L = \frac{N}{4}\sqrt{3}a_0$. And the energy dispersion is described as

$$\varepsilon^s(k,\theta) = s\gamma_0\sqrt{1 + 4cos^2\left(\frac{ka}{2}\right) + 4\cos\left(\frac{ka}{2}\right)\cos(\theta)}, \qquad (3)$$

where k is the wave vector along edge and θ is the phase angle that is perpendicular to the edge [67]. Similar to armchair nanoribbons, the energy of zigzag nanoribbons depends on wave vector k and phase angle θ. The Brillouin zone of zigzag nanoribbons only cover a quarter of that of graphene; however, it contains two independent Dirac points (K and K'), which is different from that of armchair nanoribbons. The two Dirac points are located at (k, θ) = ($\frac{2\pi}{3a}$, π) and (k, θ) = ($\frac{4\pi}{3a}$, π), as shown in figure 1.8 (b)

Production

Several methods have been introduced to produce graphene nanoribbons, including lithographic pattering (with widths down to ~20 nm) [68,69], chemical (with width 20-300 nm) [70,71,72] and sonochemical (with width down to ~10 nm)

[73], as well as unzipping of carbon nanotubes (with width down to ~1nm) [74,75,76]. However, until now, it is still a big challenge to precisely obtain high quality graphene nanoribbons with controllable widths and smooth edges. For example, graphene nanoribbons made from unzipping of carbon nanotubes are always heavily oxidized because of extensive oxidation during the unzipping process [76]. And as mentioned earlier, edges play an important role in defining the electronic properties of graphene nanoribbons, and even a few extra carbon atoms could alter their whole property. A recent discovery by scientists from UCLA and Tohoku University found out a new self-assembly method that could produce defect-free zigzag nanoribbons with periodic patterns along its edges by basically modifying the reaction between precursor molecules when they generate graphene nanoribbons patterns on the copper substrate [77]. And by using this new technique, they could control the nanoribbons' edge configuration, location and length on the substrates. And it is believed that this new method of graphene fabrication would be a stepping-stone toward the production of self-assembled graphene devices, and will largely improve the performance of the current electronic devices.

CHAPTER II

NONLINEAR DYNAMICS IN GRAPHENE UNDER AN APPLIED ELECTRIC FIELD

Introduction and Outline

The goal of this section is to study the nonlinear effects in graphene when it is exposed to an electric field. We start our discussion with the optical Bloch equations, where we visualize the dynamics of electrons coupled to an electric field in graphene, and the generation of the photon echo signals in graphene when exposed to a 90-degree excitation pulse and a 180-degree refocusing pulse. Then, we analyze the nonlinearity in graphene through the induced electric current and the harmonic generation.

Time-dependent Dirac equations

In general, the low energy quasiparticles in graphene can be accurately described by the 2+1 dimensional Dirac equation due to its symmetric crystal structure. Here, there are six Dirac points in the first Brillouin zone (as shown in figure 1.3) of graphene, but only two of them are non-equivalent, and they are

defined as K and K'. The Dirac-like Hamiltonian around the Dirac point K can be written as

$$\widehat{H}_K = v_F \vec{\sigma} \cdot \vec{p} = v_F \begin{pmatrix} 0 & \pi^+ \\ \pi & 0 \end{pmatrix} = v_F \begin{pmatrix} 0 & p_x - ip_y \\ p_x + ip_y & 0 \end{pmatrix} \quad (4)$$

while the Dirac like Hamiltonian around Dirac point K' is

$$\widehat{H}_{K'} = v_F \vec{\sigma} \cdot \vec{p} = v_F \begin{pmatrix} 0 & -\pi^+ \\ -\pi & 0 \end{pmatrix} = v_F \begin{pmatrix} 0 & -p_x + ip_y \\ -p_x - ip_y & 0 \end{pmatrix} \quad (5)$$

where $v_F \approx 10^6\ m\ s^{-1}$ is the Fermi velocity, p_x and p_y are the electron momentums in the x and y direction, respectively, and $\vec{\sigma}$ is denoted as the pseudospin of the

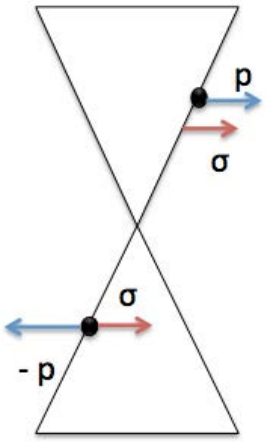

Figure 2.1. The relationship between pseudospin and momentum. The pseudospin is parallel (antiparallel) to the electron momentum in the conduction (valence) band.

carbon sublattices A and B [78,79]. The pseudospin is linked to the direction of electron propagation with its direction parallel (antiparallel) to the electron momentum in the conduction (valence) band [80], as shown on Figure 2.1. As

mentioned earlier, the energy dispersion of graphene consists of two bands: valence and conduction bands. In the undoped condition, the valence band is completely filled while the conduction band is empty. However, when an electric field E(t) is applied to graphene lattice, electrons within the valley will start moving from valence band to conduction band. The dynamics of these charge carriers are governed by the time dependent Dirac equation (TDDE) as

$$i\hbar\frac{\partial}{\partial t}\psi = v_F\begin{pmatrix} 0 & pe^{-i\phi} + eA(t) \\ pe^{i\phi} + eA(t) & 0 \end{pmatrix}\psi \quad (6)$$

where p is the magnitude of the momentum ($\vec{p} = p(cos\phi, sin\phi)$), ϕ is defined as the directional angle and is given by $\phi = \tan^{-1}(\frac{p_x}{p_y})$, e denotes the elementary charge, $A(t) = -\int E(t)dt$ is the vector potential of the field, and the two-component wave function ψ represents pseudospin from the two sublattices [79]. Equation 6 has both positive and negative solutions. The negative (electrons) solution with associated eigenvectors is expressed as

$$\psi_+(t) = \frac{1}{\sqrt{2}}\exp[-i\Omega(t)]\begin{pmatrix} e^{-\left(\frac{i}{2}\right)\theta(t)} \\ e^{\left(\frac{i}{2}\right)\theta(t)} \end{pmatrix} \quad (7)$$

and the positive solution(holes) is

$$\psi_-(t) = \frac{1}{\sqrt{2}}\exp[+i\Omega(t)]\begin{pmatrix} e^{-\left(\frac{i}{2}\right)\theta(t)} \\ -e^{\left(\frac{i}{2}\right)\theta(t)} \end{pmatrix} \quad (8)$$

where we define temporal phase $\Omega(t)$ as $\Omega(t) = \frac{v_f}{\hbar}\int \sqrt{[p_x + e\,A(t)]^2 + p_y^2}dt$, and $\theta(t)$ as the directional angle, and is given by $\Omega(t) = \tan^{-1}(\frac{p_x + e\,A(t)}{p_y})$.

Optical Bloch Equations

The optical Bloch equations are used to describe the population transfer between the energy levels, which include both population difference (n) and optical coherence (ρ). In this thesis, we focus on the simplest atomic model, which is the two-level system. And the wavefunction for this system is expressed as

$$\psi(t) = c_+(t)\,\psi_+(t) + c_-(t)\psi_-(t) \qquad (9)$$

where c_+ and c_- are the coefficients for the probability of population for the upper and lower states, respectively. Inserting Equation 7, 8, and 9 into Equation 6, it yields equations for the expansion coefficient $c_\pm$, and the resulting differential equations are written as [79]

$$\dot{c_\pm} = \frac{\iota}{2}\dot{\theta}(t)c_\mp(t)e^{\pm 2i\Omega(t)} \qquad (10)$$

From the coefficients c_+ and c_-, it is straightforward to obtain the population difference $n = |c_+|^2 - |c_-|^2$(where $|c_+|^2$ is the probability of electrons being in the upper state and $|c_-|^2$ is the probability of electrons being in the lower state) and the optical coherence $\rho = c_+c_-^*$ (is the probability of electrons in a coherent

superposition state), and the corresponding equations in the differential forms can be written as [79]:

$$\dot{n} = -i\dot{\theta}(t)\rho(t)e^{-2i\Omega(t)} \qquad (11)$$

$$\dot{\rho} = -\frac{i}{2}\dot{\theta}(t)n(t)e^{2i\Omega(t)} \qquad (12)$$

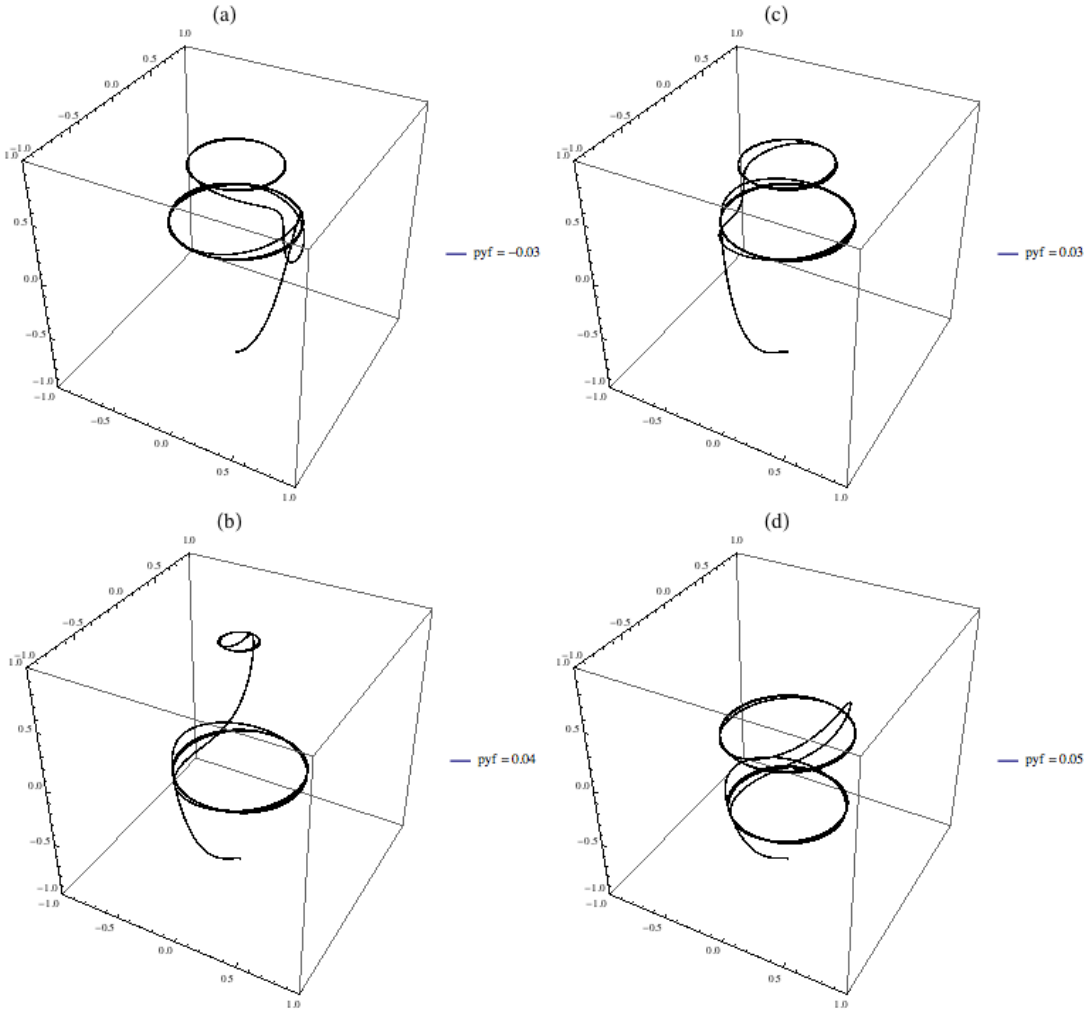

Figure 2.2. Time evolution of the Bloch vector in graphene calculated using the optical Bloch equations (11) and (12) with four different sets of values (pxf, pyf) = (-0.75, -0.03), (-0.75, 0.03), (-0.75, 0.04), and (-0.75, 0.05). Here, plots (a), (b), (c) and (d) corresponds to points (a), (b), (c) and (d) in Figure 2.3.

The solutions of the optical Bloch equations above represent the time evolution of the Bloch vector on the Bloch sphere. Here the Bloch vector ($\bar{r}$) is defined by three components: Re(ρ), Im(ρ), and n, and all these components depend on the probability of population on the upper and lower states [81]. For instance, the vectors $\bar{r}$ = (0, 0, 1) and (0, 0, -1) represent the upper and lower states as they point at the north and south poles. The time evolution of the Bloch vector in graphene under an applied electric field is depicted in Figure 2.2. Here, four points on the same energy level (shown in Figure 2.3) are picked to implement the tracing paths. Note that electrons initially start at the middle bottom of the cubic, where we define the initial values n = -1 (as in the undoped situation, we assume that all the electrons

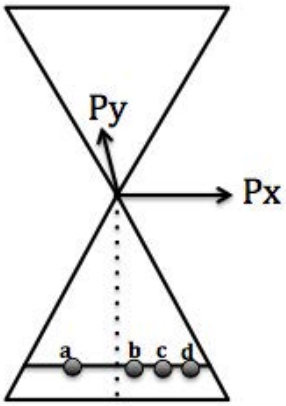

Figure 2.3. Four electrons on the same energy level are picked to implement the moving paths from the lower state to the upper state. Here points (a), (b), (c) and (d) correspond to plots (a), (b), (c) and (d) in Figure 2.2.

are concentrated at the lower state, and the upper state is completely empty), and evolve from the lower state to upper state on the Bloch sphere as time passes by. Furthermore, two electrons with the same energy level and are symmetric with respect to py=0, tend to have similar moving path but in the opposite direction, which can be seen in Figure 2.2 (a) and (b).

Photon Echoes

The evolution of photon dynamics in graphene can be observed when it is subject to an electromagnetic field. In general, photon echo dynamics consists of two

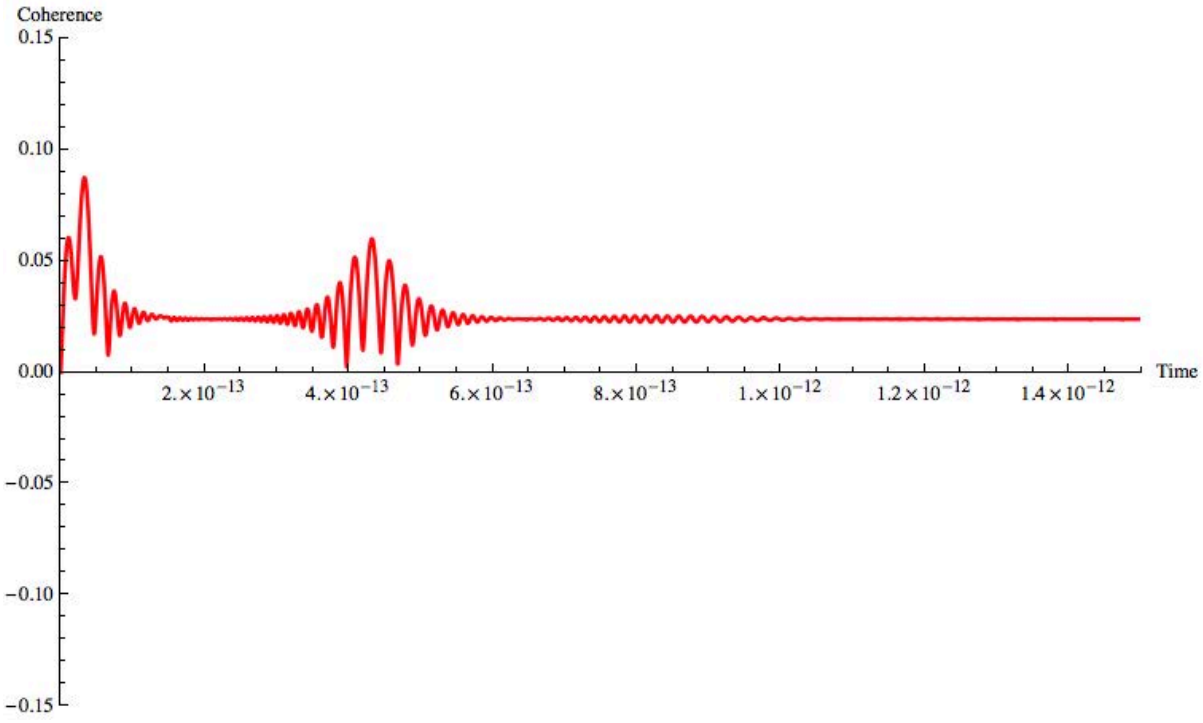

Figure 2.4. The echo signal of graphene produced with a 90-degree excitation pulse followed by a 180-degree refocusing pulse.

processes [82]. First, apply a 90-degree excitation pulse to a media, where all the photons are flipped into the horizontal plane and dephasing due to the magnetic field inhomogeneities. Then, apply a 180-degree refocusing pulse to the media to reverse all the dephasing photons into rephasing mode to generate the maximum signal. In this thesis, we focus on the evolution of photon polarization for graphene in the same manner. Here, we expose the graphene superlattice to a 90-degree excitation pulse followed by a 180-degree refocusing pulse. The produced echo signal is schematically shown in Figure 2.4. Note that the produced signal begins with a FID (free induction decay) where the signal decreases exponentially. Then after a short period, a 180-degree pulse occurs, where the signal increases to the middle point then decays exponentially. Finally, the echo signal occurs after the 180-degree pulse.

Nonlinear response in the induced current

The induced electric current for a single electron in graphene can be obtained by using the derived optical Bloch equations [79], and they are written as follows:

$$j_x = v_F\left[n\cos\theta + i\sin\theta\left\{\rho e^{-2i\Omega} - c.c.\right\}\right] \qquad (13)$$

$$j_y = v_F\left[n\sin\theta - i\cos\theta\left\{\rho e^{-2i\Omega} - c.c.\right\}\right] \qquad (14)$$

where the first and second terms represent the intraband and interband transitions, respectively. Here, one can observe very strong nonlinear response in j_x by setting n = -1 and ρ = 0, and the expression for j_x is simplified to

$$j_x = v_F \frac{p_x + e\,A(t)}{\sqrt{[p_x + e\,A(t)]^2 + p_y^2}} \qquad (15)$$

where it shows strong nonlinearity when |e A(t)|>| p_x|, | p_y|. Moreover, Equation 13 and 14 show oscillatory behavior with respect to the incident pulse since both of them have $e^{-2i\Omega}$ terms.

The current densities for the whole electron distribution are similar to the ones for the single electron, and they are expressed as [79]

$$j_x = v_F\left[(n+1)\,cos\theta + i\sin\theta\left\{\rho e^{-2i\Omega} - c.c.\right\}\right] \qquad (16)$$

$$j_y = v_F\left[(n+1)\,sin\theta - i\cos\theta\left\{\rho e^{-2i\Omega} - c.c.\right\}\right] \qquad (17)$$

Note that the current in the y direction always equal to 0 since the momentum distribution is symmetric with respect to p_y = 0. The total current can be calculated by taking the integral of the current density, which is written as

$$J(t) = -\frac{g_s g_v e}{(2\pi\hbar)^2}\int j(t)dp \qquad (18)$$

where g_s and g_v are defined as the spin and valley degeneracy factors.

Harmonic Generation

In this part, we demonstrate the nonlinear effects in graphene through the harmonic generation. Here, we plot the evolution of harmonic intensity spectrums for graphene with varying electric field strengths using the harmonic intensity spectrum equation

$$I(w) \propto \left|w\hat{J}(w)\right|^2 \qquad (19)$$

and they are schematically depicted in Figure 2.5. As shown, the strong nonlinearity in graphene can be clearly observed, where spectrums for interband transitions only, intraband transitions only and total currents change by an increase in incident field strength. At the field strength of 27.5 kV/cm, the 13th order of harmonic generation is generated. Furthermore, the nonlinearity in graphene is enhanced due to the interband transition. This is illustrated in Figure 2.5 (at the field strength of 10^{12}), where the peak of the total current curve is shifted down a little compared to the pure intraband transition.

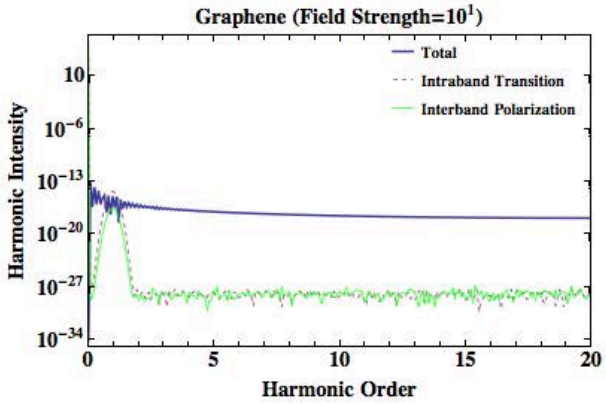
Graphene (Field Strength=10^1)
Total
Intraband Transition
Interband Polarization
Harmonic Intensity
Harmonic Order

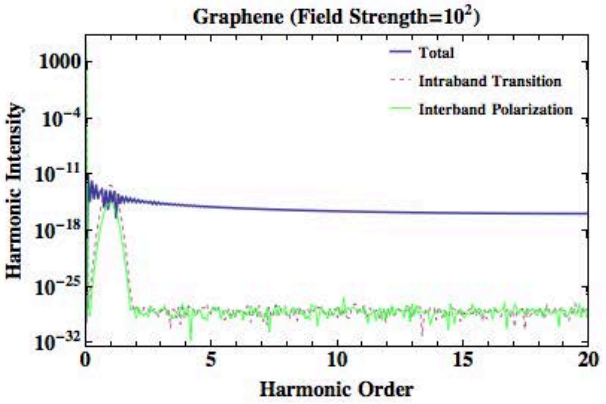
Graphene (Field Strength=10^2)
Total
Intraband Transition
Interband Polarization
Harmonic Intensity
Harmonic Order

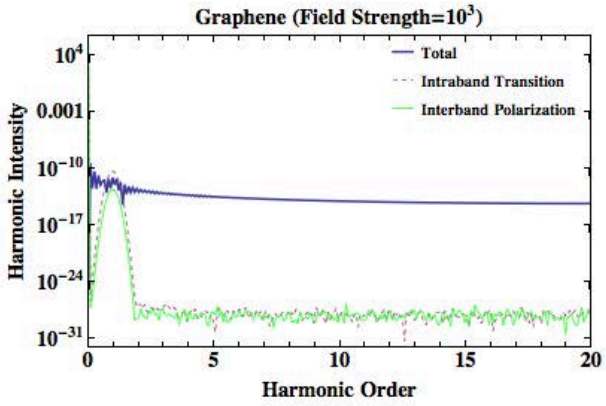
Graphene (Field Strength=10^3)
Total
Intraband Transition
Interband Polarization
Harmonic Intensity
Harmonic Order

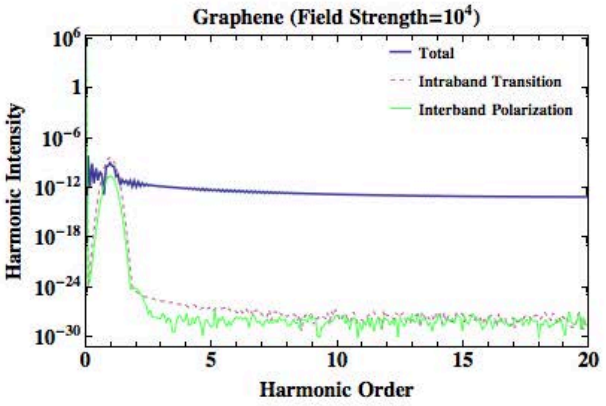
Graphene (Field Strength=10^4)
Total
Intraband Transition
Interband Polarization
Harmonic Intensity
Harmonic Order

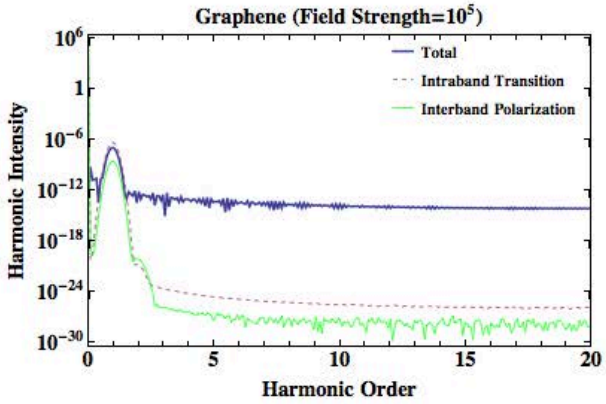
Graphene (Field Strength=10^5)
Total
Intraband Transition
Interband Polarization
Harmonic Intensity
Harmonic Order

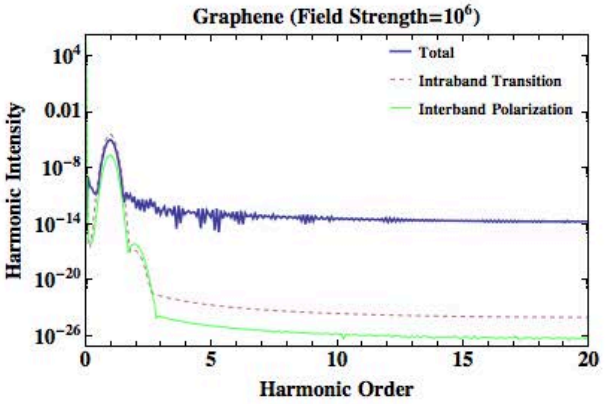
Graphene (Field Strength=10^6)
Total
Intraband Transition
Interband Polarization
Harmonic Intensity
Harmonic Order

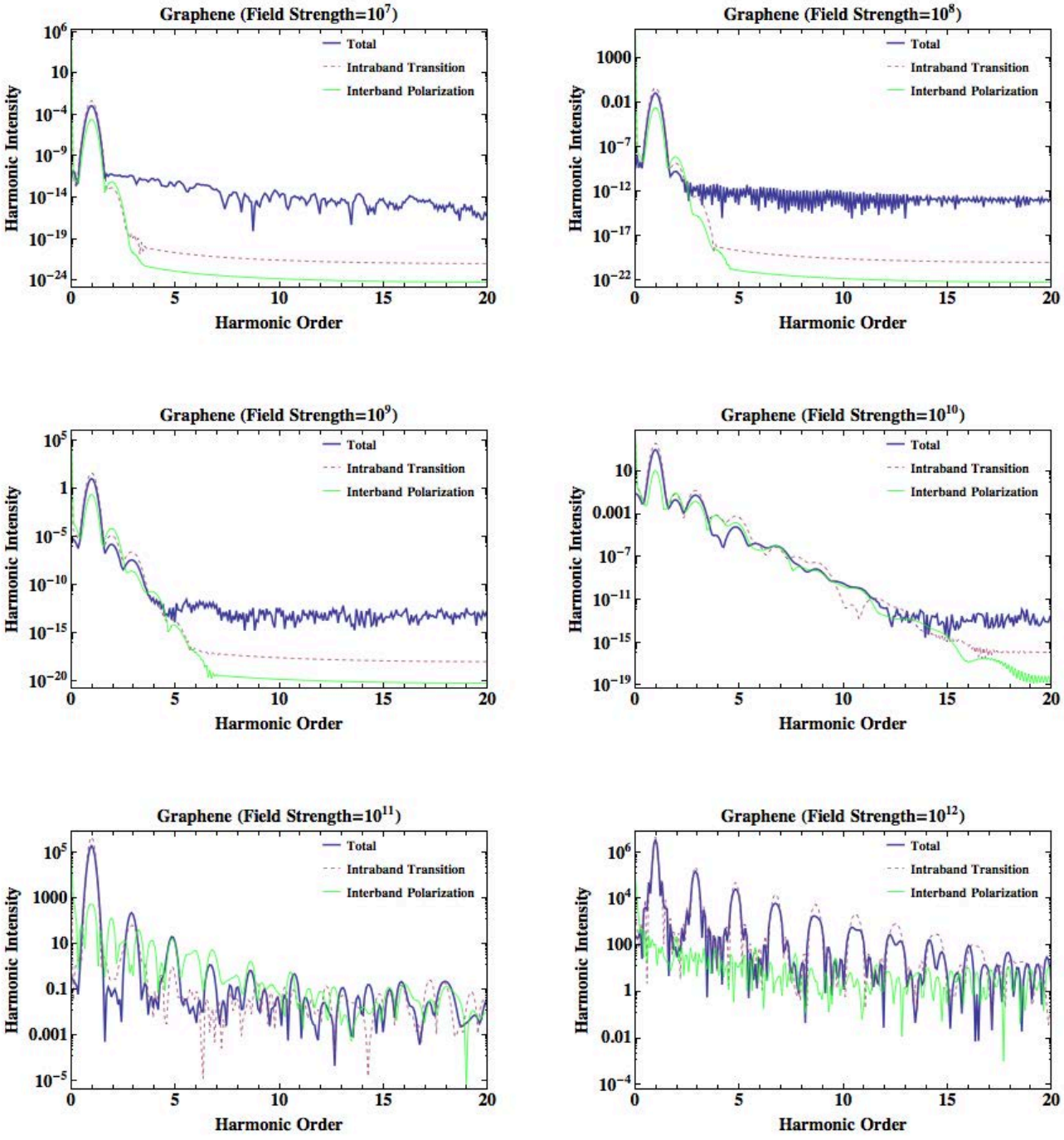

Figure 2.5. The evolution of harmonic intensity spectrums for graphene with varying electric field strengths. At the field strength of 27.5 kV/cm, the 13th order of harmonic generation is generated.

CHAPTER III

SUMMARY

Summary of Results

We began our discussion by showing the derivation of the extended optical Bloch equations from the time-dependent Dirac equations. By using these derived optical Bloch equations, we were not only able to visualize the coupling of light and field interaction under an applied electromagnetic field in graphene, but we also were able to examine the photon echo signals generated in graphene when exposed to a 90-degree excitation pulse and a 180-degree refocusing pulse.

Following our discussion of the optical Bloch equations, we theoretically proved that the induced optical absorption in graphene involves two processes: interband and intraband transitions, both of which engender nonlinearities in the terahertz range. The result of this can be clearly visualized in Figure 2.5, where spectrums for interband transitions only, intraband transitions only, and total currents change by an increase in incident field strength.

The derived current density equations consist of both interband and intraband terms, which reveals that the highly nonlinear response in graphene is

not caused solely by interband transitions or intraband transitions, but the interplay between the two transitions. This result has also been confirmed in Figure 2.5, where the spectrums for intraband transition only underwent a large change when the field strength was increased. This increase is expected because the interband injection of carriers increases the carrier densities in the conduction band. In addition, as the field strength increased, the enhancement found in the interband transitions led to the reduction in nonlinearity in the electric current in graphene. This is due to the fact that the enhanced interband dynamics smooth the abrupt change in current that was caused from the intraband dynamics. Finally, we showed that the interplay between the interband and intraband dynamics induced large harmonics in graphene, where harmonics of up to the 13^{th} order were generated.

REFERENCES

[1] Nick Bilton. (2014, Apr.) The New York Times. [Online]. http://bits.blogs.nytimes.com/2014/04/13/bend-it-charge-it-dunk-it-graphene-the-material-of-tomorrow/?_r=0

[2] A. K. Geim and K.S. Novoselov, "The rise of graphene," *Nature Materials*, vol. 6, no. 183, 2007.

[3] A. K. Geim, "Graphene: Status and Prospects," *Science*, vol. 324, no. 5934, p. 1530, June 2009.

[4] Yuanbo Zhang et al, "Experimentla Observation of the quantum Hall effect and Berry's phase in graphene," *Nature*, vol. 438, pp. 201-204, Sepetember 2005.

[5] M Scarselli et al, "Electronic and Optoelectronic nano-devices based on carbon nanotubes," *Journal of Physics: Condensed Matter*, vol. 24, no. 31, 2012.

[6] L.G. Wade, *Organic Chemistry (5th Edition)*.: Prentice Hall, 2002.

[7] M.M.Glazov and S.D.Ganichev, "High frequency electric field induced nonlinear effects in graphene," *Physics Reports*, vol. 535, no. 101, October 2013.

[8] K.S. et al Novoselov, "Two-dimensional gas of massless Dirac fermions in graphene," *Nature*, vol. 438, no. 7065, pp. 197-200, Nov. 2005.

[9] A.H.Castro Neto et al, "The electronic properties of graphene," *Rev.Mod.Phys*, vol. 81, no. 109, Jan. 2009.

[10] F. Bonaccorso et al, "Graphene photonics and optoelectronics," *Nature Photonics*, vol. 4, pp. 611-622, Aug. 2010.

[11] Sandeep Kumar Vashist and A.G. Venkatesh, "Advances in Graphene-Based Sensors and Devices," *J Nanomed Nanotechol*, vol. 4, no. 127, Nov. 2012.

[12] Nihar Mohanty and Vikas Berry, "Graphene-Based Single-Bacterium Resolution Biodevice and DNA Transistor: Interfacing Graphene Derivatives with Nanoscale and Microscale Biocomponents," *Nano Lett*, vol. 8, no. 12, pp. 4469-4476, November 2008.

[13] Kuila T, "Recent advances in graphene-based biosensors," *ncbi*, vol. 26, no. 12, pp. 4637-48, August 2011.

[14] S.A.Mikhailov, "Non-linear electromagnetic response of graphene," *EPL*, vol. 79, no. 2, June 2007.

[15] M.Dragoman et al, "Millimeter-wave generation via frequency multiplication in graphene," *Appl. Phys. Lett*, vol. 97, Aug. 2010.

[16] Jesse J. Dean and Henry M. van Driel, "Second harmonic generation from graphene and graphitic films," *Appl. Phys. Lett*, vol. 95, Dec. 2009.

[17] L.I. Magarill, and D.L.Shepelyansky M.V. Entin, "Theory of resonant photon drag in monolayer graphene," *Phys. Rev.*, vol. 81, Apr. 2010.

[18] J. Karch et al, "Dynamic Hall Effect Driven by Circularly Polarized Light in a Graphene Layer," *Phys. Rev. Lett*, vol. 105, Nov. 2010.

[19] S.A.Milkhailov, "Theory of the nonlinear optical frequency mixing effect in graphene," *Physica E: Low-dimesional Systmes and Nanostructures*, vol. 44, no. 6, Mar. 2012.

[20] Dong sun et al, "Coherent Control of Ballistic Photocurrents in Multilayer Epitaxial Graphene Using Quantum Interference," *Nano Letters*, vol. 10, no. 4, Mar. 2010.

[21] Signe Brewster. (2013, July) GIGAOM. [Online]. https://gigaom.com/2013/07/12/researchers-create-optical-switch-with-graphene-semiconductor-could-boost-internet-speeds/

[22] Huan Wang et al, "Structure-Dependent All-Optical Switching in Graphene-Nanoribbon-Like Molecules: Fully Conjugated Tri(perylene bisimides)," *J.Phys.Chem*, vol. 114, no. 34, Aug. 2010.

[23] Zhi-Bo Liu et al, "Broadband all-optical modulation using a graphene-corvered microfiber," *Laser Phys. Lett*, vol. 10, no. 6, June 2013.

[24] N.Liaros et al, "Nonlinear Optical Properties and Broadband Optical Power Limiting Action of Graphene Oxide Collids," *J. Phys. Chem*, vol. 117, no. 13, pp. 6842-50, Mar. 2013.

[25] Panit Chantharasupawong et al, "Optical Power Limiting in Fluorinated

Graphene Oxide: An Insight into the Nonlinear Optical Properties," *J. Phys. Chem.*, vol. 116, no. 49, pp. 25955-25961, Nov. 2012.

[26] S.A.Mikhailov, "Non-linear graphene optics for terahertz applications," *Microelectronics Journal* , vol. 40, no. 2009, pp. 712-715, Aug. 2008.

[27] Mike Orcutt. (2013, Oct.) MIT Technology Review.

[28] Fengnian Xia and Phaedon Avouris Thomas Mueller, "Graphene photodetectors for high-speed optical communications," *Nature Photonics*, vol. 4, pp. 297-301, Mar. 2010.

[29] Michiel.J.A. de Dood, "Second-harmonic generation," Huygens Laboratorium, 2006.

[30] Subhash Mahajan, *Encyclopedia of Materials: Scince and Technology*, K.H.J.Buschow et al, Ed.: Pergamon, 2001, vol. 10.

[31] Leandro M Malard et, "Observation of intra- and inter-band transitions in the transient optical response of graphene," *New Journal of Physics* , vol. 15, Jan. 2013.

[32] Berardi Sensale-Rodriguez et, "Broadband graphene terahertz modulators enabled by intraband transitions," *Nature Communications*, Apr. 2012.

[33] N.M.R.Peres, "Colloquium: The transport properties of graphene: An introduction," *Rev. Mod. Phys*, vol. 82, no. 2673, Sep. 2010.

[34] Chang-Hua Liu, "Graphene photodetectors with ultra-broadband and high responsivity at room temperature," *Nature Nanotechnology*, vol. 9, pp. 273-278, Mar. 2014.

[35] F.H.L.Koppens et, "Photodetectors based on graphene, other two-dimensional materials and hybrid systems," *Nature Nanotechnology*, vol. 9, pp. 780-793, Oct. 2014.

[36] Ming Liu et, "A graphene-based broadband optical modulator," *Nature*, vol. 474, pp. 64-67, May 2011.

[37] Lee et C.-C, "Broadband graphene electro-optic modulators with sub-wavelength thickness," *Optics Express*, vol. 20, no. 5, pp. 5264-5269, Feb. 2012.

[38] Nils Krane, "Preparation of Graphene," 2011.

[39] Doug Speight, "High Quality, Scalable Graphene Production," U.S. Department of Energy, Oak Ridge National Laboratory,.

[40] Luyao Zhang and Chongwu Zhou Yi Zhang, "Review of Chemical Vapor Deposition of Graphene and Related Applications," *Acc. Chem. Res.*, vol. 46, no. 10, pp. 2329-2339, Mar. 2013.

[41] Andrew James Strudwick et, "Chemical Vapor Deposition of High Quality Graphene Films from Carbon Dioxide Atmospheres," *ACS Nano*, vol. 9, no. 1, pp. 31-42, Nov. 2014.

[42] Xuesong Li et, "Large-Area Graphene Single Crystals Grown by Low-Pressure Chemical Vapor Deposition of Methane on Copper," *J.Am.Chem.Soc.*, vol. 133, no. 9, pp. 2816-2819, Feb. 2011.

[43] Mustafa Lotya et, "Liquid Phase Production of Graphene by Exfoliation of Graphite in Surfactant/Water Solutions," *J. Am. Chem. Soc.*, vol. 131, no. 10, pp. 3611-3620, Feb. 2009.

[44] Yenny Hernandez et, "High-yield production of graphene by liquid-phase exfoliation of graphite," *Nature nanotechnology*, vol. 3, no. 9, pp. 563-568, 2008.

[45] G. Gutierrez et, "Multi-layer graphene obtained by high temperature carbon implantation into nickel films," *Elsevier*, vol. 66, pp. 1-10, Jan. 2014.

[46] Dexter Johnson. (2014, May) IEEE Spectrum. [Online]. http://spectrum.ieee.org/nanoclast/semiconductors/materials/graphene-grown-directly-on-insulator-substrate-

[47] K et Khaliji, "Tunabe Bandgap in Bilayer Armchair Graphene Nanoribbons: Concurrent Influence of Electric Field and Uniaxial Strain," *Electron Devices (IEEE)*, vol. 60, no. 8, June 2013.

[48] BN Szafranek et, "Electrical observation of a tunable band gap in bilayer graphene nanoribbons at room temperature," *Applied Physics Letters*, vol. 96, no. 11, 2010.

[49] Liying Jiao et, "Narrow graphene nanoribbons from carbon naotubes," *Nature*, vol. 458, pp. 877-880, Apr. 2009.

[50] Liming Xie et, "Graphene Nanoribbons from Unzipped Carbon Nanotubes: Atomic Structure, Raman Spectroscopy, and Electrical Properties," *J. Am. Chem. Soc*, vol. 133, no. 27, pp. 10394-10397, June 2011.

[51] Sankaran, Stephan Roche, and Gianaurelio Cuniberti Lakshmi, "Spin-valve effect in zigzag graphene naoribbons by defect engineering," *Physical Review B*, vol. 80, no. 19, 2009.

[52] Fatemeh Ostovari and Mohammad Kazem Moravvej-Farshi, "Dual function armchair graphene nanoribbon-based spin-photodetector: Optical spin-value and light helicity detector," *Appl. Phys. Lett*, vol. 105, Aug. 2014.

[53] Heidelberg. (2014, Apr.) Springer. [Online]. http://www.springer.com/about+springer/media/springer+select?SGWID=0-11001-6-1460343-0

[54] Shu Nakaharai et, "Gate-Controlled P-I-N Junction Switching Device with Graphene Nanoribbon," *Applied Physics Express*, vol. 5, 2012.

[55] Feras Al-Dirini and Efstratios Skafidas Faruque M. Hossain, "A graphene naoribbon neuro-sensor for glycine detection and imaging," *J. Appl. Phys.*, vol. 115, June 2014.

[56] Son JG et, "Sub-10 nm Graphene Nanoribbon Array field-effect transistors fabricated by bloch copolymer lithography," *Adv Mater.*, vol. 25, no. 34, pp. 4723-8, Sep. 2013.

[57] A.Y. et Goharrizi, "Device Performance of Graphene Nanoribbon Field-Effect Transistors in the Presence of Line-Edge Roughness," *Electron Devices (IEEE)*, vol. 59, no. 12, pp. 3527-3532, Oct. 2012.

[58] Yihua Xue et, "N-doped graphene nanoribbons as efficient metal-free counter electrodes for disulfide/thiolate redox mediated DSSCs," *Nanoscale*, vol. 10, Jan. 2015.

[59] Klemen Pirnat et, "Redox-Active Functionalized Graphene Nanoribbons as Electrode Material for Li-Ion Batteries," *ChemElectroChem*, vol. 1, no. 12, pp. 2131-2137, Nov. 2014.

[60] Chao Xie et, "Schottky solar cells based on graphene nanoribbon/multiple silicon nanowires junctions," *Appl. Phys. Lett.*, vol. 100, May 2012.

[61] P.B. Mendonca and A. R. Rocha Cesar E.P. Villegas, "Optical spectrum of bottom-up graphene nanoribbons: towards efficient atom-thick excitonic solar cells,"

Scientific Reports, vol. 4, Oct. 2014.

[62] Liangbo Liang and Vincent Meunier, "Atomically Precise Graphene Nanoribbon Heterojunctions for Excitonic Solar Cells," *J. Phys. Chem. C*, vol. 119, no. 1, Dec. 2014.

[63] Yu Ye et, "Multicolor graphene nanoribbon/semiconductor nanowire heterojunction light-emitting diodes ," *J. Mater. Chem.*, vol. 21, pp. 11760-11763, July 2011.

[64] Meisam Rahmani et, "Monolayer Graphene Nanoribbon p–n Junction," *Journal of Nanoengineering and Nanomanufacturing*, vol. 2, no. 4, pp. 375-378, Dec. 2012.

[65] A., and Lee, C. Kargar, "Graphene nanoribbon schottky diodes using asymmetric contacts," in *In Nanotechnology, 2009. IEEE-NANO 2009. 9th IEEE Conference on*, 2009, pp. 243-245.

[66] L. Brey and H.A. Fertig, "Electronic States of Graphene Nanoribbons," *Phys. Rev. B*, vol. 73, 2006.

[67] Ken-ichi Sasaki et, "Theory of optical transitions in graphene nanoribbons," *Phys. Rev. B*, vol. 84, Sep. 2011.

[68] L., et Tapaszto, "Tailoring the atomic structure of graphene nanoribbons by scanning tunnelling microscope lithography," *Nature nanotechnology*, vol. 3, no. 7, pp. 397-401, 2008.

[69] Sunmin Ryu et, "Raman Spectroscopy of Lithographically Patterned Graphene Nanoribbons," *ACS Nano*, vol. 5, no. 5, pp. 4123-4130, Mar. 2011.

[70] Datta et, "Crystallographic etching of few-layer graphene," *Nano Lett*, vol. 8, pp. 1912-1915, 2008.

[71] Campos-Delgado et, "Bulk production of a new form of sp(2) carbon: crystalline graphene nanoribbons," *Nano Lett*, vol. 8, pp. 2773-2778, 2008.

[72] X. Y. et Yang, "Two-dimensional graphene nanoribbons," *J. Am. Chem. Soc.* , vol. 120, pp. 4216-4217, 2008.

[73] X. L et Li, "Chemically derived, ultrasmooth graphene nanoribbon semiconductors," *Science*, vol. 319, pp. 1229-1232, 2008.

[74] D. V. et Kosynkin, "Longitudinal unzipping of carbon nanotubes to form graphene nanoribbons," *Nature*, vol. 458, pp. 872-875, 2009.

[75] A. L. et Elías, "Longitudinal cutting of pure and doped carbon nanotubes to form graphitic nanoribbons using metal clusters as nanoscalpels," *Nano Lett.*, vol. 10, pp. 366-372, 2009.

[76] L., Wang, X., Diankov, G., Wang, H. & Dai, H iao, "Facile synthesis of high-quality graphene nanoribbons," *Nature Nanotechnol*, vol. 5, pp. 321-325, 2010.

[77] Shaun Mason. (2014, Oct.) UCLA Newsroom. [Online]. http://newsroom.ucla.edu

[78] F. J. López-Rodríguez and G. G. Naumis, "Analytic solution for electrons and holes in graphene under electromagnetic waves: Gap appearance and nonlinear effects," *Physical Review B*, vol. 78, 2008.

[79] Kenichi L. Ishikawa, "Nonlinear optical response of graphene in time domain ," *Physical Review B*, vol. 82, Nov. 2010.

[80] M. I., Novoselov, K. S., & Geim, A. K. Katsnelson, "Chiral tunnelling and the Klein paradox in graphene ," *Nature physics*, vol. 2, no. 9, pp. 620-625, 2006.

[81] Jose Mawyin and Harold Metcalf. Simulation of Optical Bloch Equations for two and three level atoms. [Online]. http://laser.physics.sunysb.edu/~jose/Bloch2.pdf

[82] E. L. Hahn, "Spin Echoes," *Phys. Rev.*, vol. 80, no. 580, Nov. 1950.

[83] D. V. et Kosynkin, "Longitudinal unzipping of carbon nanotubes to form graphene nanoribbons," *Nature*, vol. 458, pp. 872-875, 2009.

[84] A. L. et Elias, "Longitudinal cutting of pure and doped carbon nanotubes to form graphitic nanoribbons using metal clusters as nanoscalpels," *Nano Lett.*, vol. 10, pp. 366-372, 2009.